https://ntrs.nasa.gov/search.jsp?R=19770012632 2020-03-22T11:35:42+00:00Z

N77-19576 Not on
NASA CR-145134

FINAL REPORT

PHASE II

Optimization of Solar Cells for Air Mass Zero Operation and a Study of Solar Cells at High Temperatures

NASA Contract - NASI-12812

Principal Investigators - H. Hovel, J. M. Woodall

Work Performed by
Exploratory Materials and Devices Project
IBM Research Laboratory
Yorktown Heights, New York

Final Report Covering the Period
Jan. 20, 1975 - March 1, 1976

REPRODUCIBLE COPY
(FACILITY CASEFILE COPY)

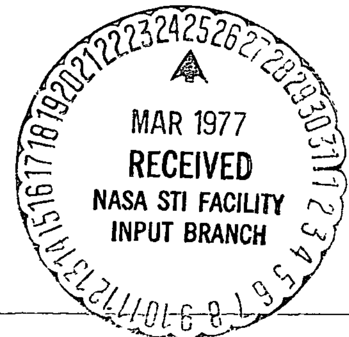

National Aeronautics and Space Administration

OPTIMIZATION OF SOLAR CELLS FOR AIR MASS ZERO OPERATION AND A STUDY OF SOLAR CELLS AT HIGH TEMPERATURE

By H. J. Hovel and J. M. Woodall
IBM Thomas J. Watson Research Center
Yorktown Heights, New York 10598

I. OBJECTIVE

The purpose of this contract is to develop crystal growth procedures, fabrication techniques, and theoretical analysis in order to make GaAlAs-GaAs solar cell structures which exhibit high performance at: 1) Air Mass 0 illumination and 2) high temperature conditions.

II. LIQUID PHASE EPITAXIAL GROWTH EXPERIMENTS

During this period, most of the liquid phase epitaxy (LPE) experiments were aimed at the p-$Ga_{1-x}Al_xAs$, p-GaAs, n-GaAs structure in which the target thickness and composition of the $Ga_{1-x}Al_xAs$ layer was 0.25-0.5μ and X = 0.85 respectively. Previously[1] several cells of this type were made with a $Ga_{1-x}Al_xAs$ layer thickness of 0.6-0.9μ. Even though these cells showed the expected improved spectral response,[2] there were several problems which prevented the realization of cells with AMO efficiencies of 18% or greater. One problem was the large series resistance of the cells. It was felt that this could be solved by using both a better contact metallurgy and a post growth Zn diffusion. The other problem was the reproducible growth of uniform layers of $Ga_{1-x}Al_xAs$ which were 0.25-0.5μ thick. The layers on the previous cells were still too thick and non-uniform to produce high efficiency

cells. Therefore, an effort was made to develop growth procedures to achieve the desired results. In the previous report[1], there is much detail concerning many aspects of the LPE procedures used in this work. Consequently, only the procedures new to this work will be described here.

The starting point for this work is the use of crucible 3 and the growth schedule of Fig. 4 from Ref. 1. There are several reasons for this. First, the previously used crucible (#2 Ref. 1) with the BN inserts was highly deteriorated. It was felt, based on the "leaching effect"[1], that the use of high purity Poco graphite would not have a detrimental effect on the cells. The initial use of the growth schedule in Fig. 1 was predicated on the fact that this produced the best previous run, SCB62.[1]

The operational procedure of the poco graphite fixture differed from that of the BN fixture. In addition the purge gas lines were modified to reduce water and oxygen contamination. The most significant change was to make the hydrogen gas pass through an oxysorb unit just ahead of a high vacuum shut off valve at the entrance to the LPE system. This allows evacuation and backfill of the system with a reduced chance for oxygen and water contamination because the gas receives a final purification prior to entering the LPE system.

The important changes in the operation of the graphite fixture from the BN fixture was that the Al was inserted into a solidified Ga melt after an overnight bake at 900°C in hydrogen. In addition, a GaAs source bar was located on top of the melt. As before, a GaAs "lead" or "wipe" bar was placed just ahead of the GaAs substrate. It turned out that the GaAs source bar on top of the melt produced dramatic changes in the morphology of the $Ga_{1-x}Al_xAs$. Characteristically, there were a few nucleated areas which grew into rather large island type structures which were smoothly faceted. In between there was no evidence for any growth which exceeded 500Å in thickness.

After nine runs, in which several growth parameters were varied, (see SCL 1-9, Table I), it was determined that the top source bar contributed to non-uniform growth. As a result it was hypothesized that in order to produce smooth, thin film heteroepitaxy, it is necessary for the $Ga_{1-x}Al_xAs$ melt to be supersaturated at the instant of contact with the GaAs substrate. This results in the formation of a high density of nuclei which rapidly join together forming a smooth continuous film free from low index plane, e.g., (100), faceting. Continued supersaturation of the melt produces a uniform diffusion boundary layer which maintains a smoothly moving solid-liquid interface. In the case where both a top source bar and lead bar was used this resulted in a nearly equilibrium melt which caused a low density of nuclei and a highly faceted island type surface structure. Thus, fast cooling rates or supercooled melts should consistently yield smooth films provided the substrate and melt are free from nucleation inhibitors such as oxides.

Several growths were made without the use of a top source bar. The best results occurred when the growth schedule did not include a "leaching" step. This result revealed a fundamental problem: in order to make good cells from GaAs n-type substrates with average or poor hole diffusion lengths (l_p, 0.5-1μ) it has been found necessary for them to be in contact with equilibrium Ga-Al-As:Zn melts for at least ten minutes before growth of the $Ga_{1-x}Al_xAs$ layer. However, in order to grow smooth $Ga_{1-x}Al_xAs$ layers, it was found that the melt must be supersaturated before substrate contact. Unfortunately, this condition will cause immediate growth upon substrate melt contact and, hence, no leaching seems likely to occur. If it is supposed that leaching will occur <u>after</u> the $Ga_{1-x}Al_xAs$ layer is grown, it is possible to devise a

growth schedule in which the substrate contacts a supersaturated Ga-Al-As:Zn melt such that the re-equilibration of the melt produces the required thickness of the $Ga_{1-x}Al_xAs$ layer. Subsequently, the substrate plus growth is allowed to remain in contact with the melt for "leaching". Several growths were made to test the post growth leaching hypothesis (see SCL 12-17, Table I). In these runs, the melts were supercooled from 0.5 to 2.0°C prior to substrate contact. After contact, the substrate plus growths were leached from 25 to 60 minutes. The results were only partially encouraging. Even though substrates were usually entirely covered with a $Ga_{1-x}Al_xAs$ layer, one end of the wafer usually had a thicker growth than the other. Also, the end with the thinner growth was rougher than the thick end. This was determined to be caused by an etching effect by the melt on the substrate due to thermal gradients along the substrate. At the hotter end, the GaAs substrate gets etched away. The saturated melt at the hotter end diffuses to the colder and where it becomes supersaturated. This results in the growth of $Ga_{1-x}Al_xAs$. Since non-uniform layers are undesirable, adjustments were made in the growth apparatus to eliminate the temperature gradients. It was noted that even though the GaAs substrate may be etched by the melt, it is still covered by a thin $Ga_{1-x}Al_xAs$ layer after the run. Thus, even after adjustment of the apparatus, it was decided that an intentional etchback of the GaAs substrate prior to growth might be beneficial for the cell. A series of runs (see SCL 20-30, 33-35, Table I) were performed in which after the substrate made contact with a saturated melt, the temperature was raised 3 to 5°C. This makes the melt undersaturated which in turn causes etchback of the substrate until the melt becomes saturated again. The melt and substrate are maintained isothermal for about 30 minutes. The substrate is then separated from the melt and the run terminated.

This procedure has produced the most promising results to date. First, the surface of growths is not mirror smooth. However, the $Ga_{1-x}Al_xAs$ layer is uniform and undulating over the entire wafer. Even though the surface is undulating, it is covered by a $Ga_{1-x}Al_xAs$ layer which is 0.2-0.5μ thick over the entire surface, and the p-n junction follows the etchback contour of the GaAs surface. The desirability of this structure is shown in Fig. 2, the spectral response of a cell (SCL-30) made by the upheat technique. Note both the uniform response at low photon energies and the large photocurrent tail at high photon energies. This suggest that the minority carrier diffusion lengths in the substrate have been improved and that the thickness of the $Ga_{1-x}Al_xAs$ layer is less than 0.5μ. Another beneficial aspect of this growth method was demonstrated by depth profiling of the $Ga_{1-x}Al_xAs$ layer using sputter etching and Auger analysis. It was found that the layer was graded in composition from pure GaAs at the substrate surface to $Ga_{0.15}Al_{0.85}As$ at the growth surface. This produces a drift field which enhances photoexcited carrier separation in the $Ga_{1-x}Al_xAs$ layer.

There are, however, several problems with the cells made by this technique. First, the open circuit voltage, V_{oc}, is usually very low, 0.6-0.8 volts. This is associated with a large dark current, or leakage current. The source of this current is thought to be associated with defects in the p-n junction region. The second problem is either a high contact resistance or high sheet resistance leading to low fill factors. The identification and elimination of these problems will be subject of future investigations.

III. CONTACT TECHNOLOGY

Contacts to GaAlAs-GaAs solar cells have generally been made using Au-Ge-Ni or Ag-Sn to the nGaAs base, and Au-Zn or Ag-Zn to the pGaAlAs surface layer. It is necessary to sinter these contacts at temperatures of 450-525°C for five minutes in order to obtain acceptably low contact resistances. After sintering of Au-Zn contacts to devices with narrow junctions and thin GaAlAs layers, high leakage currents very often resulted, and in some cases completely shorted devices were obtained. This problem was reduced by a switch to Ag-Zn contacts, but even with these, leaky devices were often obtained. Calculations using the diffusion coefficient of Ag in GaAs indicated that the Ag could be expected to diffuse for several microns at 500°C in five minutes. Therefore, while Au-Zn and Ag-Zn might be acceptable for devices with thick GaAlAs layers and deep junctions, they were not acceptable for very thin GaAlAs layers and narrow junctions.

Therefore, a search was started for a more suitable contact metallurgy. Several good contact technologies for p-type GaAs have been previously developed including Au, Ag, In-Ag, Cr and Ti. The GaAs must be heavily doped ($> 5 \times 10^{18}$ cm^{-3}) for low contact resistances to be obtained, and contact sintering at 300-500°C must be performed. It was expected that these conditions would apply to GaAlAs as well as to GaAs.

Contact resistance measurements to both diffused and undiffused surfaces have been made using a variety of metallurgies. Most of these metallurgies were evaporated onto the sample through pattern-defining metal masks, but several electroless and electro-plating techniques were also tested. The testing configuration is shown in Fig. 3. Current is passed through the

outer two contacts. The voltage drop is measured across the inner two electrodes using a very high impedance voltmeter to eliminate any contact resistance. The contact resistance may then be measured in several ways using one or both of the current carrying electrodes.

Some measured contact resistances are shown in Table 2. Contact resistances of 4×10^{-3} ohm $-cm^2$ or less are obtained for Cr, Au, Au-Zn, Ag-Zn, or Pd on heavily doped (10^{20} cm^{-3}) surfaces. When the doping is 10^{19} cm^{-3} or less, the contact resistances are an order of magnitude or more higher for most metals. Pd, however, is an exception. Evaporated or electrolessly plated Pd gave low resistances even for doping levels as low as $2-4 \times 10^{18}$ cm^{-3}. Pd was also the only metal which gave a low contact resistance to undiffused GaAlAs, and did not require any annealing to obtain this low resistance (although annealing at 300°C or above improved the adherence considerably).

It is desirable to use the Pd as the contact to GaAlAs since this eliminates the need for an added Zn diffusion to obtain a high surface doping level. Therefore, the contact metallurgy that is used now consists of an electron-beam evaporated Pd layer about 500Å thick followed by a thicker layer (5000Å) of Al. Most samples are annealed at about 300°C in a forming gas (N_2-H_2) atmosphere to improve the adherence.

IV. HIGH TEMPERATURE SOLAR CELLS

One of the main advantages of GaAs-based solar cells is their ability to operate efficiently at high temperatures. This is mainly due to the relatively high bandgap of GaAs and the consequent high value of V_{oc}. However, other material and device parameters also partially determine the temperature

behavior of these solar cells, including the absorption coefficient, the minority carrier mobility, and the minority carrier lifetime.

The absorption coefficient of GaAs as a function of temperature is shown in Fig. 4, as compiled from the absorption data of Sturge[3] and the bandgap versus temperature dependence reported by Panish and Casey.[4] The absorption edge shifts significantly toward the infrared, increasing the long wavelength spectral response and the photocurrent. The spectral responses that would be expected for these shifts in the absorption edge but with all other parameters held constant are shown in Fig. 5.

Changes in lifetime with temperature would affect the photocurrent additionally by raising or lowering the spectral response according to the diffusion length variation. The measurements of Vilms and Spicer,[5] Kladis and Euthymiou,[6] and Dudenkova and Nikitin[7] all indicate that the minority carrier lifetime improves with increasing temperature. An example of the effect of variable diffusion lengths on the expected spectral response is shown in Fig. 5. The largest effect is seen at low temperatures where the diffusion lengths become small compared to the junction depth and the inverse of the absorption coefficient.

To determine whether the shift in absorption edge or the diffusion length variation affects the current most, the expected photocurrents for the three cases of: 1) variable α, constant L; 2) constant α, variable L; 3) both variables; were calculated and are shown in Fig. 6. The shift is absorption edge by itself would cause a concave upward increase in the photocurrent, while the variation in L by itself would cause a saturating improvement in the current. The expected variations in both quantities taken together should result in a "more-or-less" linear increase in the photocurrent with temperature.

Diffusion Length Measurements

The $Ga_{1-x}Al_xAs$-GaAs cell with its low recombination velocity at the interface can be a valuable tool for studying the variations of lifetime and diffusion length with temperature. The technique is to match the absolute response, corrected for reflection, with the predicted responses for various assumed diffusion lengths. Devices with shallow junctions yield results indicative of the hole diffusion length in the n type base region, as shown in Fig. 7. Narrow diffusion lengths yield curves (1) which improve at high photon energies, where carriers are generated closer to the interface. When the diffusion length improves with temperature to become greater than $(1/\alpha)$, the response becomes relatively flat (curve 3).

Devices with deep junctions can be used to study to electron diffusion length in p type GaAs, Fig. 8. At low temperatures, the diffusion length will not extend from the junction to the interface, and high energy generated carrier will be lost (curve 2). As the diffusion length improves, high energy generated carriers will be collected and the response will improve (curve 1).

Devices with intermediate junction depths will yield results which depend on the variations of both the hole and electron diffusion lengths.

To test these ideas on practical GaAlAs-GaAs cells, spectral response measurements were made as a function of temperature using a series of 21 narrow band pass filters and an Eppley termopile as a calibrated detector. The devices were kept in vacuum during these temperature measurements and the light was incident through a sapphire window. No devices were available having very narrow junction depths. However, a variety of cells were available with junction depths of 1μ or greater, making it possible to study the electron

diffusion length in the pGaAs very easily, and to some degree the hole diffusion length in the nGaAs base can be estimated as well.

The spectral response as a function of temperature for a cell with a 1μ junction depth and a 1μ GaAlAs layer is shown in Fig. 9. The enhanced response with increasing temperature implies improvements in both the hold and electron diffusion lengths, with the strongest variation occurring below room temperature. The computer curves which yield the best match to the measured ones are shown in Fig. 10, along with the diffusion length values used to obtain the curves. The diffusion length improvements are substantial and in good agreement with Vilms and Spicer.[5]

The measured spectral responses of a cell (SCB62) with a very deep junction are shown in Fig. 11. Again, a strong variation of the electron diffusion length with temperature is indicated. Matching computed responses to the experimental ones yield the best fit curves shown in Fig. 12. The diffusion lengths behave qualitatively the same as the Vilms and Spicer[5] results, but are slightly higher quantitatively, which might be expected due to the higher perfection of devices made by liquid phase epitaxy.

A summary of the diffusion length results as a function of temperature is shown in Fig. 13, together with other experimental results.[5,7] The GaAlAs-GaAs results agree well with those of Vilms and Spicer.[5] The variations reported in the Russian work are much smaller, but this can be easily explained as differences in the nature of the recombination centers in the two cases.

The diffusion length is a composite of the mobility and lifetime,

$$L = \frac{\kappa T}{q} \mu \cdot \tau \tag{1}$$

The mobility in GaAs is determined by both ionized impurity scattering and optical phonon scattering, and is fairly constant with temperature as a result.[8] The $(\kappa T/q)\mu$ term would therefore tend to increase the diffusion length as the square root of T. This is not enough to explain the observed increase in L, Fig. 13. Therefore, the lifetime improvement is largely responsible.

The lifetime, in a very simple approximation, is related to the density N_r of empty (filled) recombination centers in n-type (p-type) material, the thermal velocity ν_{th} ($= \sqrt{2\kappa T/m^*}$), and the capture cross-section α by

$$\tau \propto \frac{1}{N_r \, \nu_{th} \alpha} \tag{2}$$

The thermal velocity increases as $T^{1/2}$ and tends to <u>decrease</u> the lifetime with increasing T. Capture cross-sections, however, tend to either decrease[9] or remain constant[10] with increasing T, which would either <u>increase</u> the lifetime or not affect it, respectively. The density of recombination centers can change dramatically with T or remain constant. One possible example of how this could happen is shown in Fig. 14, for electron recombination in p-type material. Initially, the Fermi level lies below the shallow recombination center E_{r_1}. This center is therefore empty, able to accept electrons, and participates in the recombination process. As the temperature increases, the Fermi level moves toward the center of the gap; the centers at E_{r_1} will then begin to fill, becoming unavailable for recombination, and the lifetime will increase. If deep centers are dominant in the recombination, E_{r_2}, then the filling of the recombination levels and the lifetime will be much less affected by temperature.

Although this example may not necessarily be responsible for the measured behavior in the GaAlAs-GaAs cells, nevertheless, it demonstrates how differences in the energy depth of recombination centers along with differences in their capture cross-sections can lead to various types of diffusion length behavior with temperature as indicated in Fig. 13.

Device Measurements

The behavior of GaAs solar cells with temperature will depend on 1) the absorption edge shift of both GaAs and GaAlAs, 2) the change in diffusion length, 3) the intrinsic density n_i and its effect on V_{oc}, 4) the series resistance and its effect on the fill factor.

Past measurements[11] have shown that increasing temperatures result in decreasing V_{oc} and FF, as expected, but also that the I_{sc} increases with temperature strongly, and therefore, the efficiency is sustained to higher values with increasing temperatures than had been previously predicted.[12] The measured behavior of one cell at AMO was shown in Fig. 3 of the Quarterly Report for October 1, 1974. The measured behavior of another cell (SCB62) is shown in Fig. 15 (this report). The V_{oc} decreases linearly with temperature while the J_{sc} increases linearly. The conversion efficiency tapers gradually up to about 125°C and more sharply thereafter. The inherent efficiency (after correction for contact area) decreases from 14.5% at 25°C to 13.5% at 120°C and 8.8% at 250°C. The extrapolated value is about 6% at 300°C.

The drop in V_{oc} with temperature is a straight forward result of the increasing intrinsic carrier density n_i (and therefore increasing dark current). The increasing short circuit current is partially the result of the diffusion length and GaAs absorption edge changes with temperature. However, the measured photocurrents tend to vary more strongly with temperature than the computed ones even after taking these changes into account.

The measured currents are lower at low temperature than expected, possibly due to a stronger variation in diffusion length than expected. On the other hand, the measured currents are larger at high temperatures than expected. Part of this discrepancy is due to the higher infrared content of Xenon light compared to the AMO spectrum. Part of it could also be due to improvements in the GaAlAs collection parameters. The GaAlAs bandgap decreases with increasing temperature, which would normally tend to decrease the photocurrent. If the diffusion length increases and the surface recombination decreases at higher temperatures, though, as might be expected, then added carriers will be collected from the GaAlAs and the photocurrent will increase. In this case, a current of 42 mA/cm^2 at 600°K is computed. Spectral response measurements on devices with very thin GaAlAs layers are as yet unable to confirm whether this happens or not, but measurements on devices with 0.6μ layers or more (SCB62, Fig. 11) indicate that at these thicknesses the high energy response worsens slightly at high temperatures. The photocurrents and efficiences above 250°C in Fig. 15 are therefore probably too high by about 3-4 mA/cm^2 and 1/2-1 percentage point, respectively, due to the excess infrared content in the Xenon source.

REFERENCES

1. Hovel, H. J. and Woodall, J. M.: Optimization of Solar Cells for Air Mass Zero Operation and a Study of Solar Cells at High Temperatures. Final Report, Phase I, NASA Contract NASI-12812.

2. Hovel, H. J. and Woodall, J. M.: Optimization of Solar Cells for Air Mass Zero Operation and a Study of Solar Cells at High Temperatures. Quarterly Progress Report, NASA Contract NASI-12812, March 1975.

3. Sturge, M. D.: Optical Absorption of Gallium Arsenide between 0.6 and 2.75 eV. Phys. Rev. Lett., Vol. 127, 1962, pp. 768.

4. Panish, M. B.; and Casey Jr., H. C.: Temperature Dependence of the Energy Gap in GaAs and GaP. J. Appl. Phys., Vol. 40, 1969, pp. 163.

5. Vilms, J.; and Spicer, W. E.: Quantum Efficiency and Radiative Lifetime in p-Type Gallium Arsenide. J. Appl. Phys., Vol. 36, 1965, pp. 2815.

6. Kladis, D. I.; and Euthymiou, P. C.: Temperature Dependence of Minority Carrier Lifetime in Low Resistivity GaAs. J. Appl. Phys., Vol. 45, 1974, pp. 2775.

7. Dudenkova, A. V.; and Nikitin, V. V.: Lifetime in Single Crystals of Gallium Arsenide. Sov. Phys. Sol. St., Vol. 8, 1967, pp. 2432.

8. Hovel, H. J.: Solar Cells. Vol. II of Semiconductors and Semimetals. Academic Press (New York), 1976.

9. Hovel, H. J.; and Milnes, A. G.: The Electrical Characteristics of nZnSe-pGe Heterodiodes. Int. J. Elects., Vol. 25, 1968, pp. 201.

10. Wessels, B. W.: Temperature Dependence of Minority Carrier Lifetime in Vapor Grown GaP. J. Appl. Phys., Vol. 46, 1975, pp. 2143.

11. Hovel, H. J.; and Woodall, J. M.: $Ga_{1-x}Al_xAs$-GaAs P-P-N Heterojunction Solar Cells. J. Electrochem. Soc., Vol. 120, 1973, pp. 1246. Also, Hovel, H. J.; and Woodall, J. M.: Optimization of Solar Cells for Air Mass Zero Operation and a Study of Solar Cells at High Temperatures. Quarterly Progress Report, NASA Contract NASI-12812, October, 1974.

12. Wysocki, J. J.; and Rappaport, P.: Effect of Temperature on Photovoltaic Solar Energy Conversion. J. Appl. Phys., Vol. 31, 1960, pp. 571.

TABLE I List of Runs and Growth Parameters

SCL Run #	gms Ga	mgm Al	C_{zn} mg/g	X*	D μ	X_j μ	T_g	ΔT °C / C.R.	Leach Time	Growth Sch Fig	Sub #	Zn Diff.	Comments
1	2.0	28.2	14.1	0.85	0.25*	1.1*	898	0.5 / 0.12	10'	4	424L	-	Nonuniform growth. Use lead bar and top source
2	2.0	28.5	14.2	0.85	0.25*	1.1*	900	0.5 / 0.12	10'	4	424L	-	"
3	2.0	28.7	14.4	0.85	0.38*	1.1	900	0.75 / 0.12	10'	4	424L	-	"
4	2.0	28.4	14.2	0.85	0.75	1.1*	895	0.75 / 0.5	0	4	424L	-	No top source bar. Use lead bar for melt
5	2.0	28.6	14.1	0.85	0.38*	1.1*	895	0.75 / 1.25	0	4	424L	-	Use top source bar for melt. Use lead bar.
6	2.0	28.3	14.1	0.85	0.75*	1.1*	895	0.75 / 0.5	0	4	424L	-	No top source bar. Use lead bar for melt.
7	2.0	28.1	14.1	0.85	1.5*	1.1*	914	1.5 / 0.5	10'	5	424L	-	" 7°C
8	2.0	28.1	14.1	-	-	1.1*	895	0.75 / 0.12	10'	4	424L	-	Test for substrate surface. No melt contact.
9	2.0	28.2	14.2	0.85	2.5	1.1*	905	1.5 / 0.12	10'	4	G1-19	700°C / 2'	No top source bar for melt. Use lead bar.
10	2.0	28.4	14.3	0.85	1.0*	1.1*	905	1.0 / 0.15	0	4	G1-19	-	"
11	2.0	28.3	14.3	0.85	0.5*	1.1*	900	0.5 / 0.10	20'	4	G1-19	-	"
12.	2.0	28.1	14.3	0.85	0.5*	1.1*	895	0.5 / 0	20'	4	G1-19	-	Super cool melt. 0.5°C before sub. contact.
13.	2.0	28.0	14.1	0.85	1.0*	1.1*	895	1.0 / 0	25'	4	G1-22	-	Super cool melt. 1.0°C before b. contact
14	2.0	28.6	14.0	0.85	1.0*	1.1*	895	1.0 / 0	30'	4	G1-22	-	"
15	2.0	28.4	14.3	0.85	1.0*	1.1*	895	1.0 / 0	25'	4	G1-22	700°C / 2'	"
16	2.5	35.0	14.0	0.85	1.0	1.1*	895	1.0 / 0	30'	4	G1-22	-	"
17	2.5	35.2	14.1	0.85	1.8	1.1*	894	0 / 0	45'	4	G1-22	-	No cooling after substrate contact

Table I (continued)

18	2.5	35.5	14.3	0.85	-	1.1*	900	-0.75/0	60'	5	G1-18	-	Undersaturate melt 0.75°C before contact.
19	2.5	35.7	14.2	0.85	-	1.1*	900	-20/0	60'	5	G1-18	-	" 2.0°C before Sub. contact
20	2.5	35.7	14.1	0.85	-	1.1*	910	-5.0/0	30'	**	G1-19	-	Melt undersaturation before sub contact
21	2.5	35.5	14.1	0.85	3.2	1.1*	909	-5.0/0	30'	**	G1-18	-	" "
22	2.5	35.6	14.1	0.85	-	1.2	910	-4.5/0	30'	**	4193	-	" "
23	2.5	35.3	14.0	0.85	-	1.1*	909	-5.0/0	30'	**	4193	-	" "
24	2.5	35.0	14.0	0.85	-	1.1*	912	-5.0/0	30'	**	4193	-	" "
25	2.5	35.1	14.1	0.85	-	1.1*	906	-4.0/0	30'	**	4193	-	" "
26	2.5	35.5	14.2	0.85	-	1.1*	906	-4.0/0	30'	**	4193	-	" "
27	2.5	35.4	14.1	0.85	-	1.1*	906	-5.0/0	30'	**	p-u-Zn-71	-	" "
28	2.5	35.0	14.1	0.85	-	1.1*	907	-5.0/0	30'	**	p-u-Zn-71	-	" "
29	2.5	35.3	14.1	0.85	-	1.1*	908	-5.0/0	30'	**	p-u-Zn-71	-	" "
30	2.5	35.2	14.1	0.85	-	1.1*	906	-5.0/0	30'	**	p-u-Zn-71	-	" "
31	2.5	35.2	14.0	0.85	0.65*	1.1*	900	0.5/0.2	0	4	p-u-Zn-71	-	Similar to SCL-6
32	2.5	35.1	14.2	0.85	0.65*	1.1*	895	0.5/1.0	0	4	p-u-Zn-71	-	" "
33	2.5	35.3	28.0	0.85	-	1.65*	906	-4.0/0	30'	**	G1-22	-	Melt undersaturation before sub. contact
34	2.5	35.1	14.2	0.85	-	1.1*	909	-5.0/0	30'	**	G1-22	-	" "
35	2.5	35.1	14.2	0.85	-	1.1*	905	-3.0/0	30'	**	G1-22	-	" "

* = Calculated values

C.R. = Cooling Rate, °C per min.

** = Melt is saturated. Substrate brought into contact with melt. Temperature of melt raised and held for 30 minutes. Substrate removed from melt.

Table 2. Contact resistances in ohm-cm^2. Annealing was for 5 minutes at temperature shown.

Material (p type)	Metal	Dope	25° C	250	350	400	450	500
GaAs	Cr-Au	10^{20}	3.5×10^{-3}	3.5×10^{-3}	3.5×10^{-3}	3.5×10^{-3}	3.5×10^{-3}	3.5×10^{-3}
GaAs	Pd*	10^{20}	2.2×10^{-3}	1.5×10^{-3}	1.5×10^{-3}			
GaAs	Aℓ-Mg	10^{19}	4.5×10^{-2}		9.3×10^{-3}	9×10^{-3}	5×10^{-3}	4×10^{-3}
GaAs	Ag-Mg	10^{19}	1.3×10^{-1}		2.3×10^{-2}	1×10^{-2}	8.9×10^{-3}	7×10^{-3}
GaAs	Cr	4×10^{18}	2.5×10^{-2}	1.3×10^{-2}	3.3×10^{-2}	2.6×10^{-1}	4×10^{-1}	
GaAs	Au**	4×10^{18}	3.8×10^{-2}	1×10^{-2}	4.1×10^{-3}	5×10^{-3}	4×10^{-2}	
GaAs	Pd*	4×10^{18}	1.6×10^{-3}	1.6×10^{-3}	1.6×10^{-3}			
GaAs	Pd***	4×10^{18}	3.0×10^{-3}					
GaAℓAs (85% Aℓ)	Au-Mg	2×10^{18}	52	52	52	52	49	11
	Aℓ-Mg	2×10^{18}	624	481	294	204	56	33
	Cr-Au	5×10^{19}	1.4	1.3	1.1	1.2	1.1	1.1
	Pd-Aℓ	2×10^{18}	10^{-2}					

*Electroless plated

**Electroplated

***Evaporated

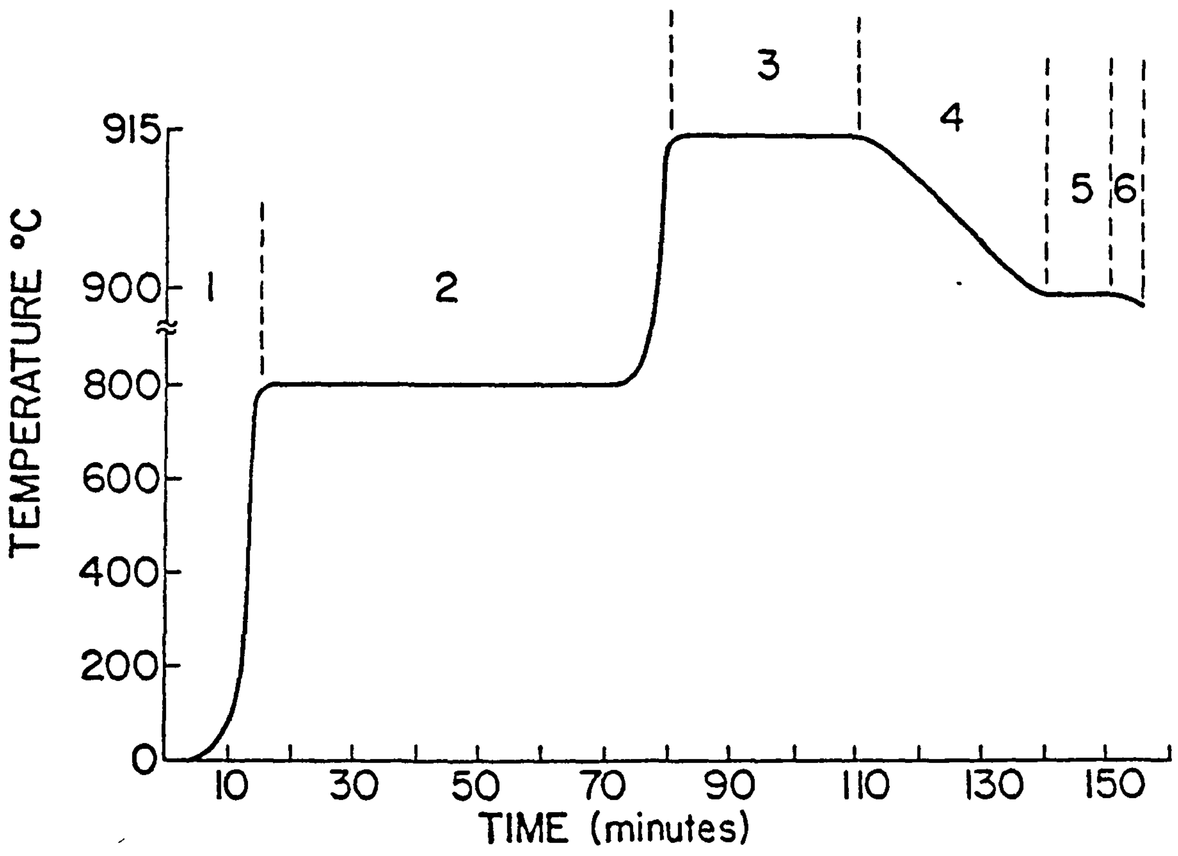

FIGURE 1 - Growth Schedule for Liquid Phase Epitaxy

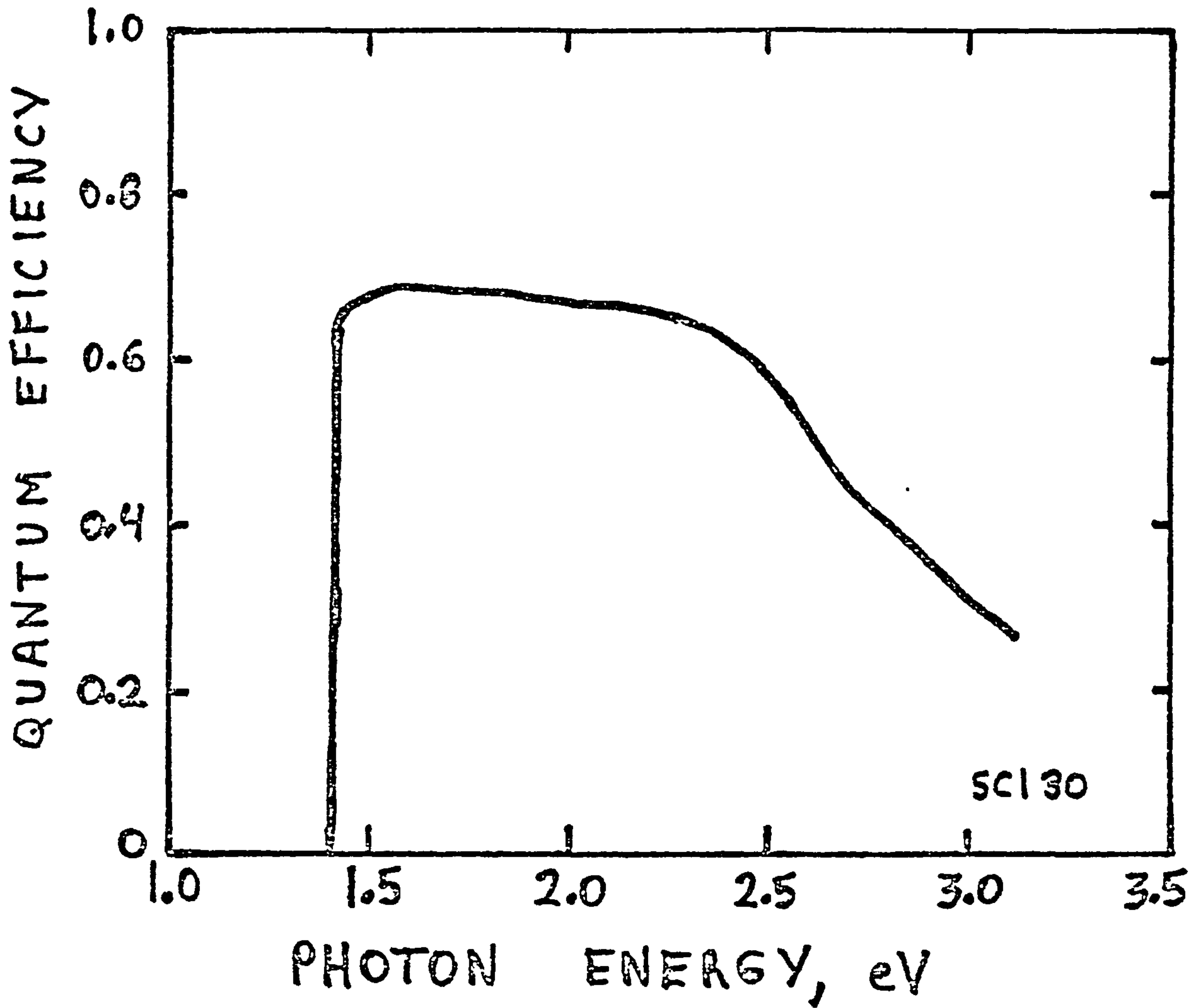

Figure 2 Spectral response of a recent solar cell made by the saturated melt technique and contacted without Zn diffusion using evaporated Pd. (No anti-reflection coating)

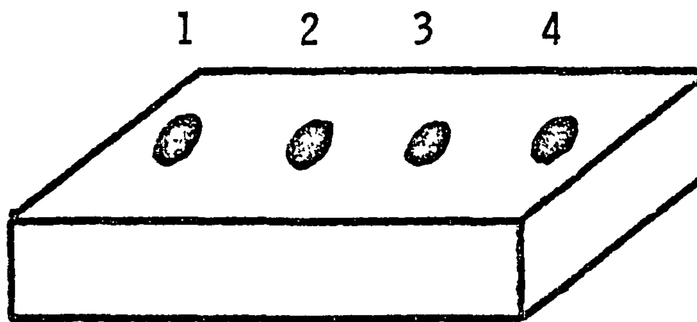

$$R_{bulk} = V_{23} / I_{14}$$

$$2\,R_{contact} = (V_{14} / I_{14}) - 3\,R_{bulk}$$

Figure 3

Configuration for Resistance Measurement

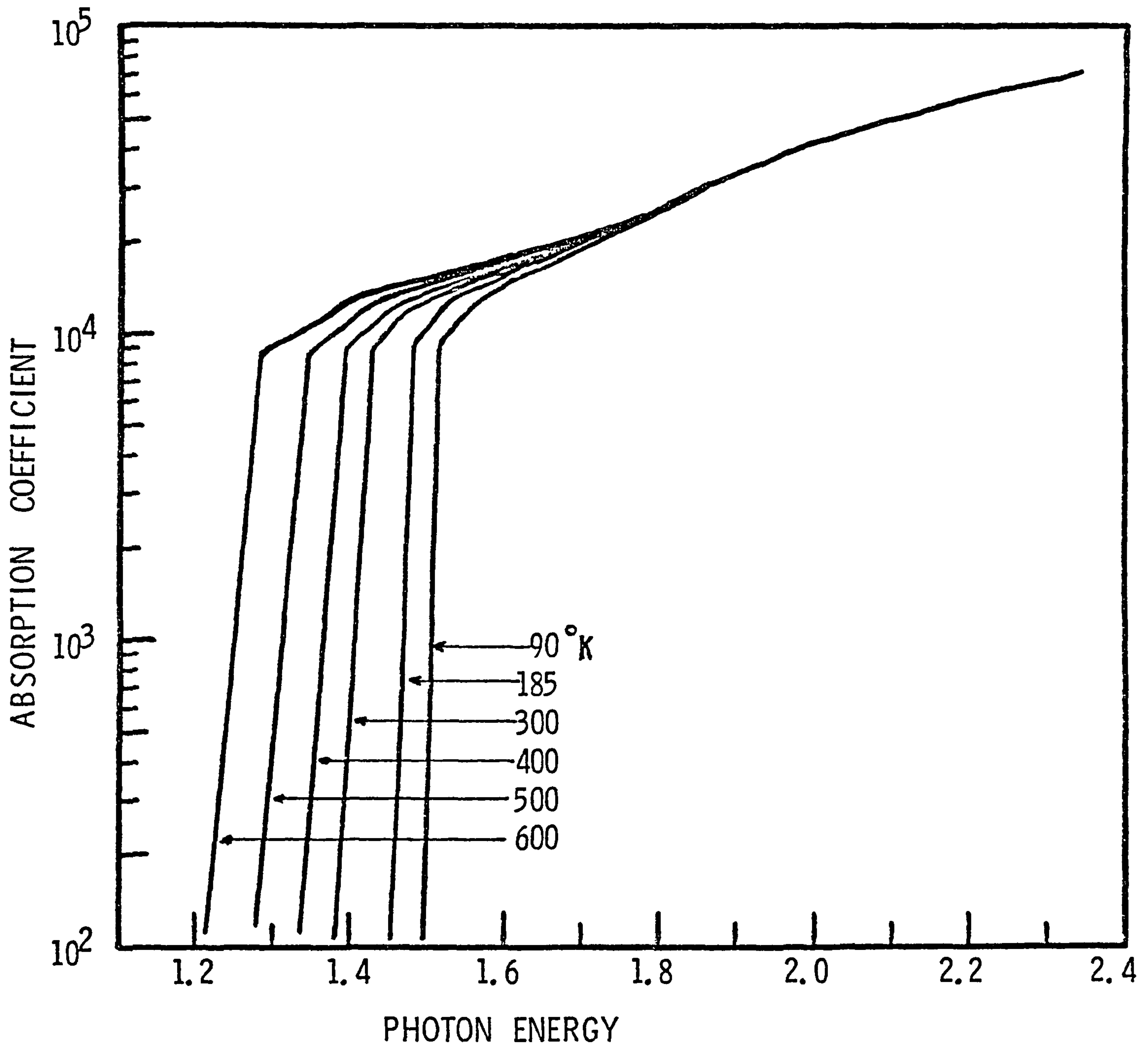

ABSORPTION COEFFICIENT OF GaAs versus TEMPERATURE

Figure 4

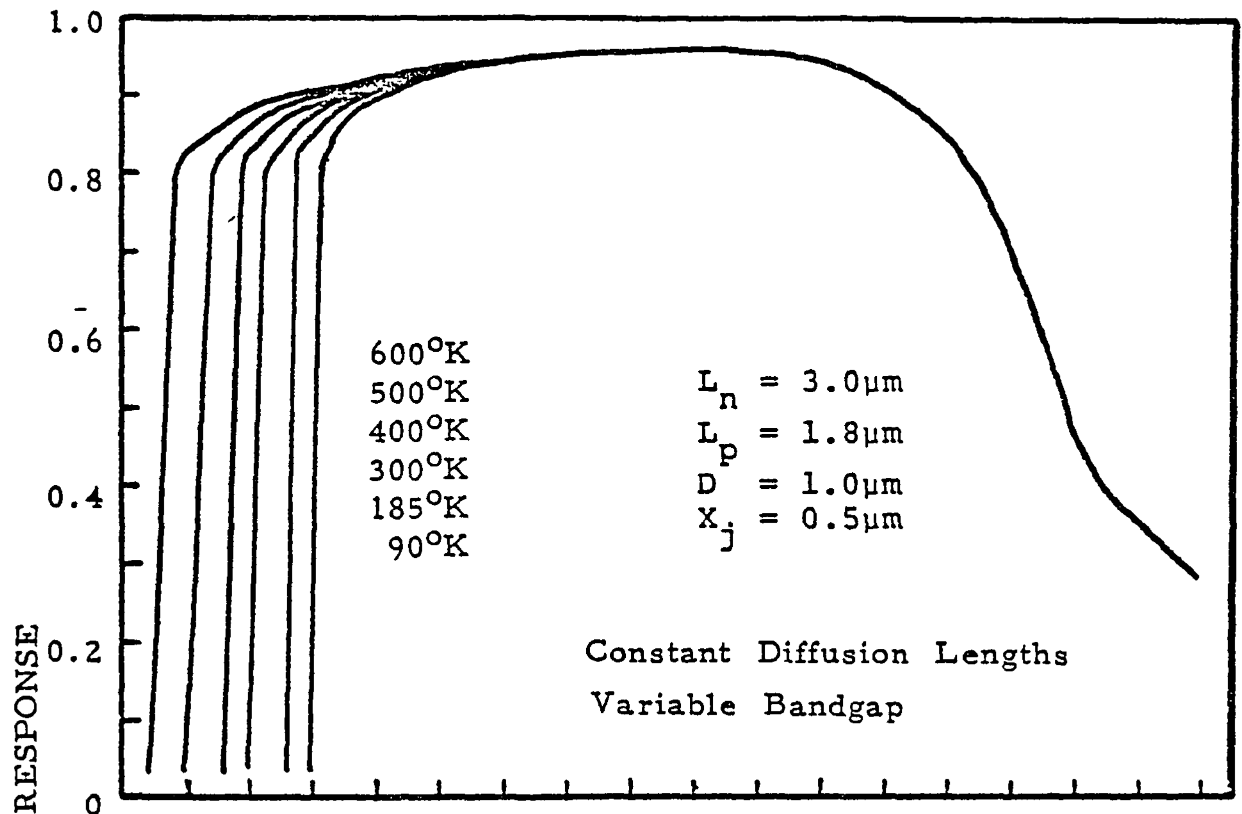

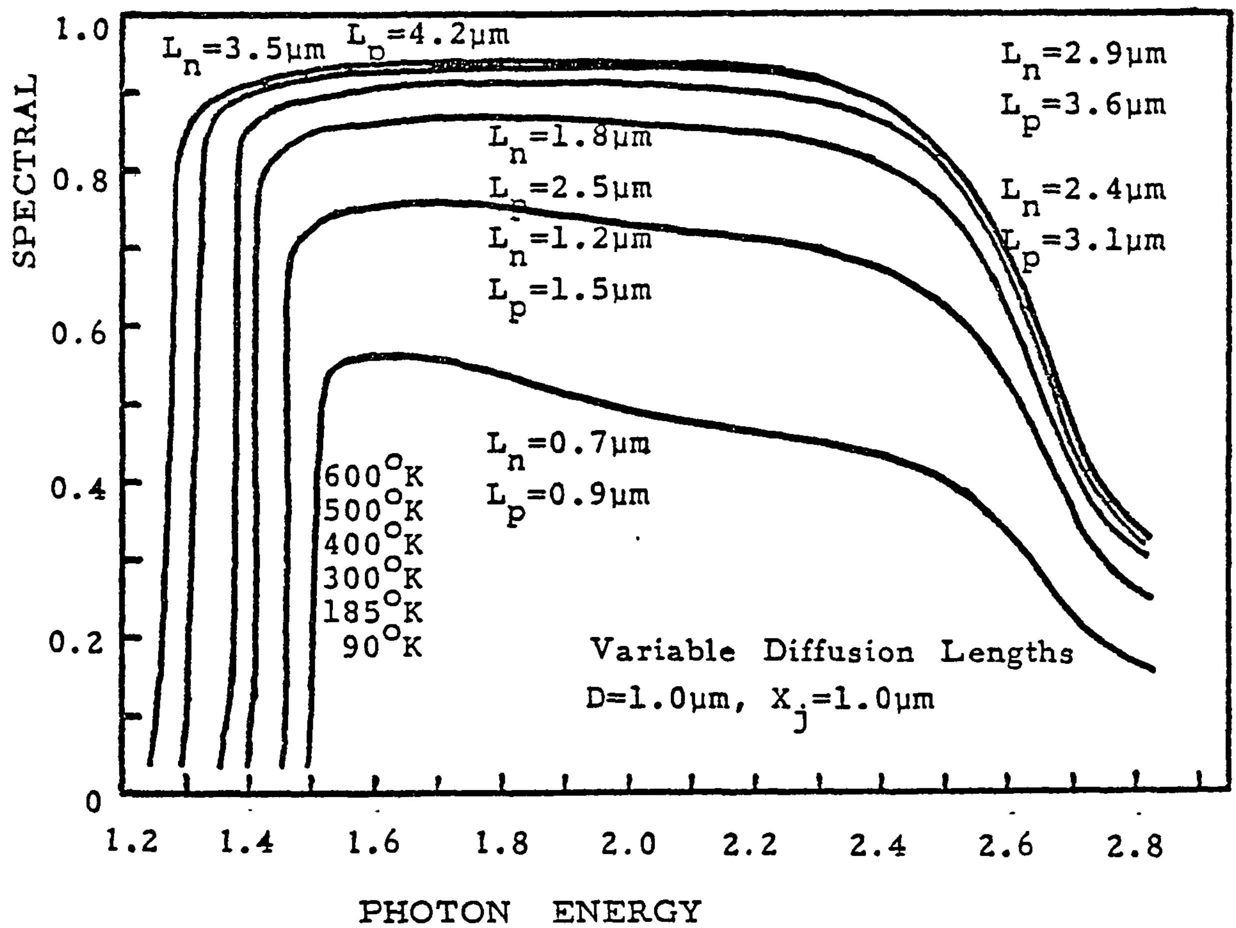

Calculated spectral responses for two conditions

Figure 5

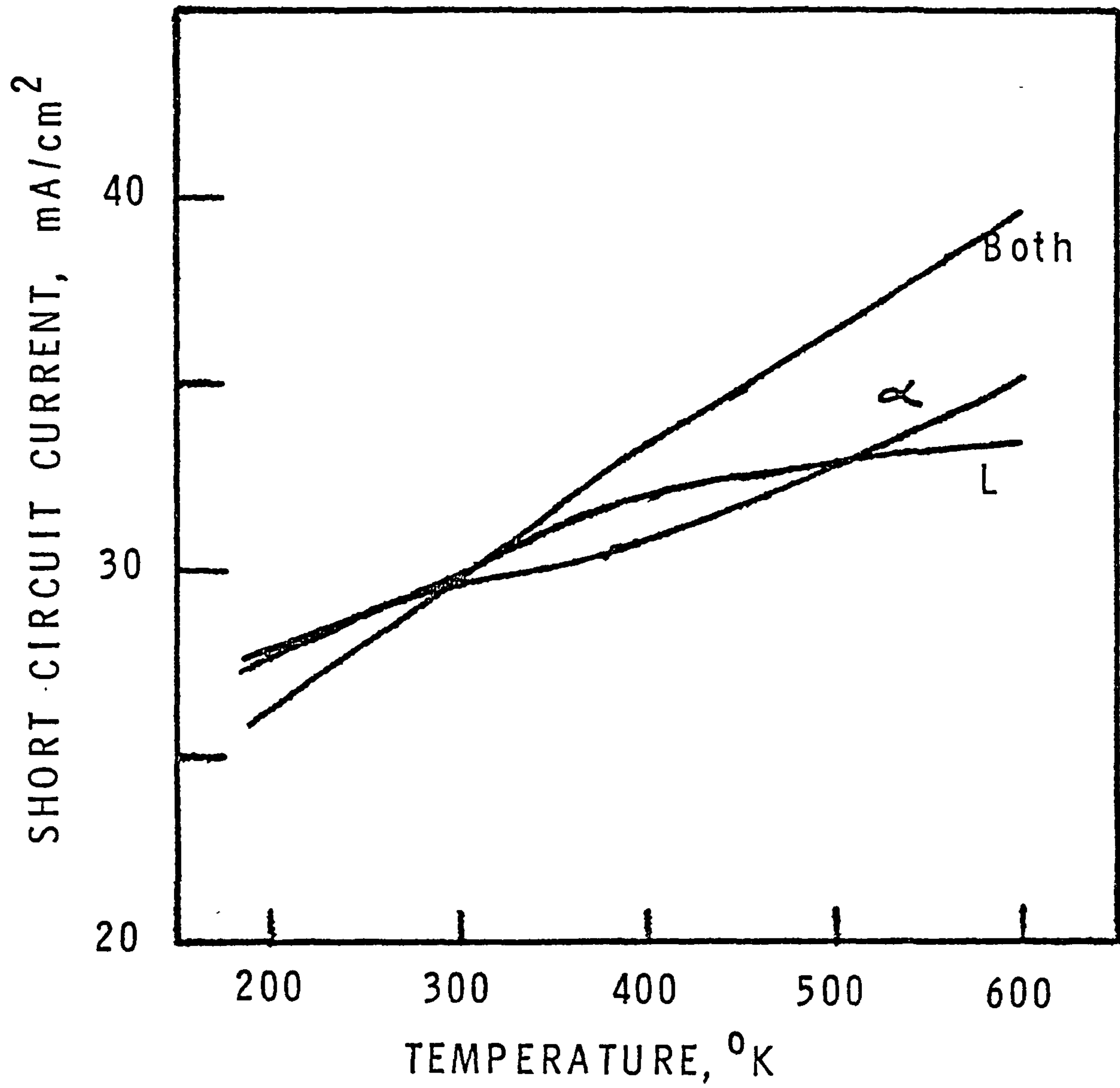

Variation in J_{sc} at AM0 for: 1) α variable, 2) L variable, 3) both variable.

Figure 6

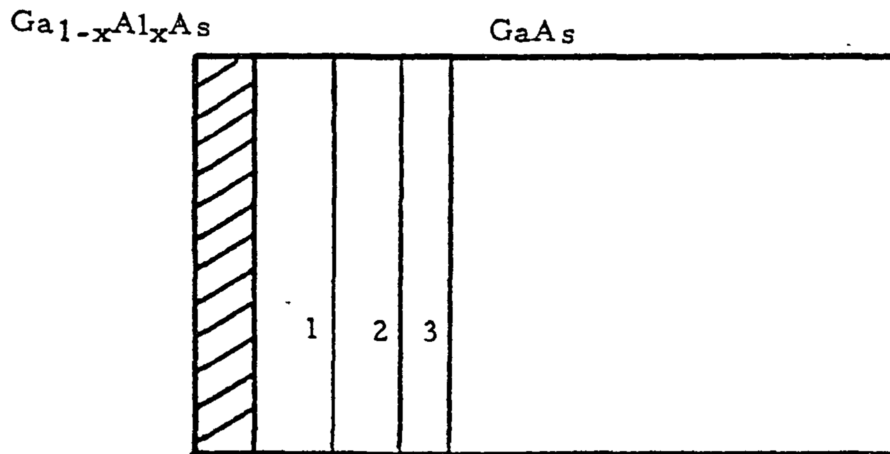

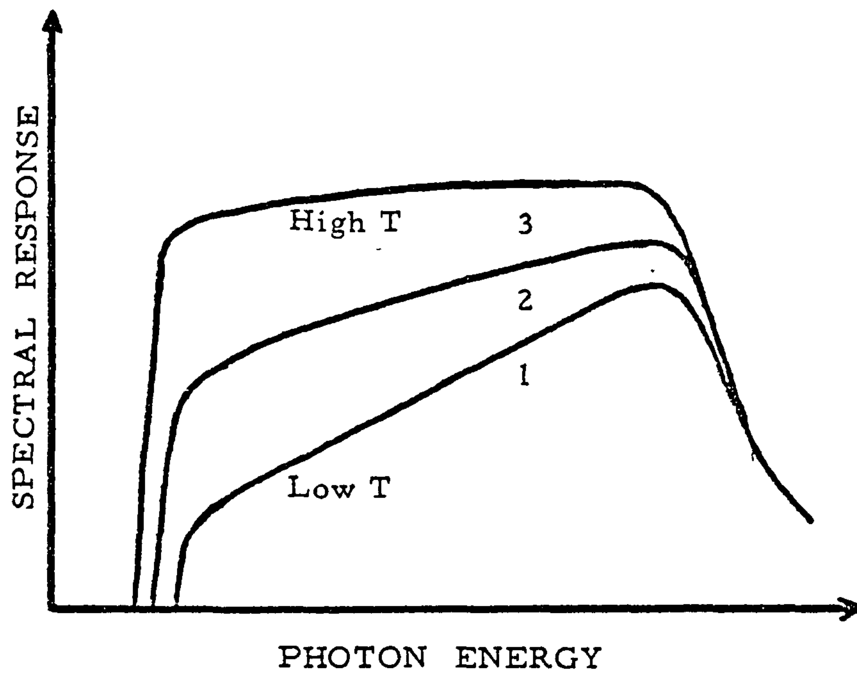

DEVICES WITH SHALLOW JUNCTIONS

Figure 7

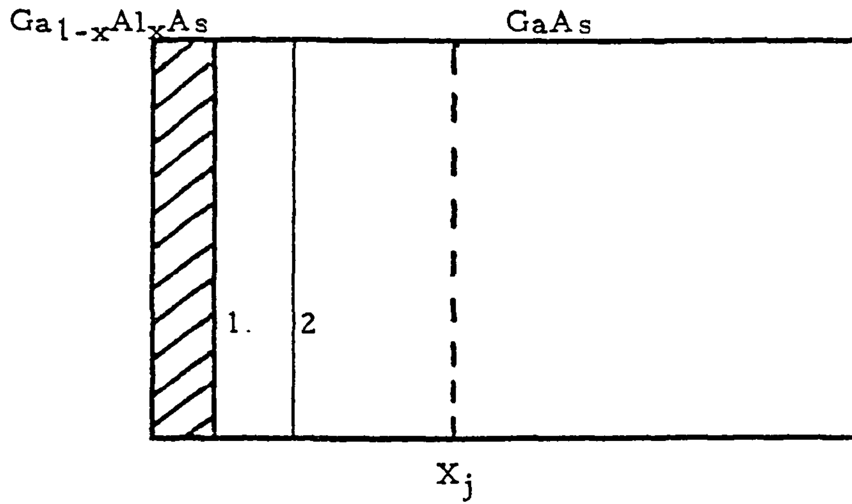

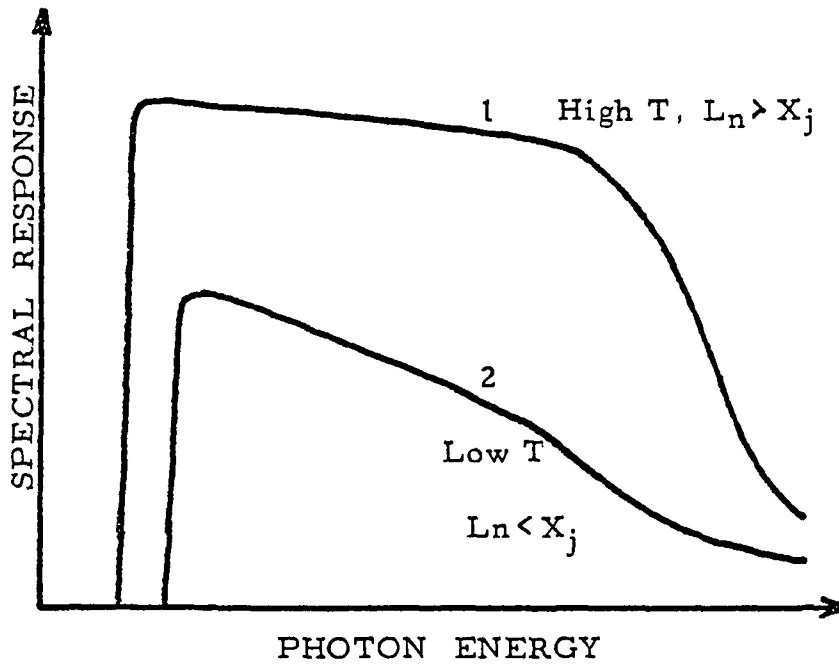

DEVICES WITH DEEP JUNCTIONS

Figure 8

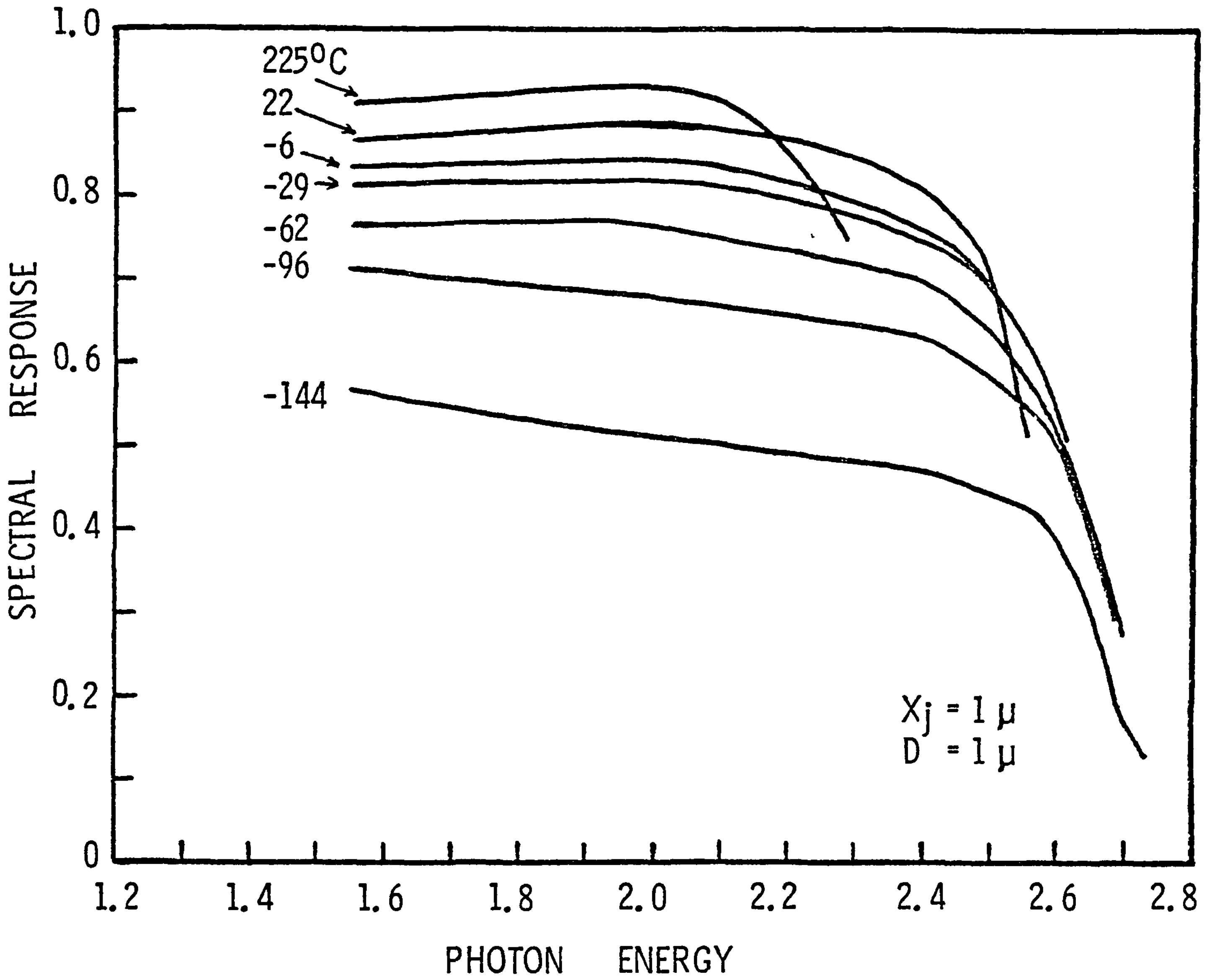

MEASURED RESPONSES OF A CELL WITH MODERATE JUNCTION DEPTH

Figure 9

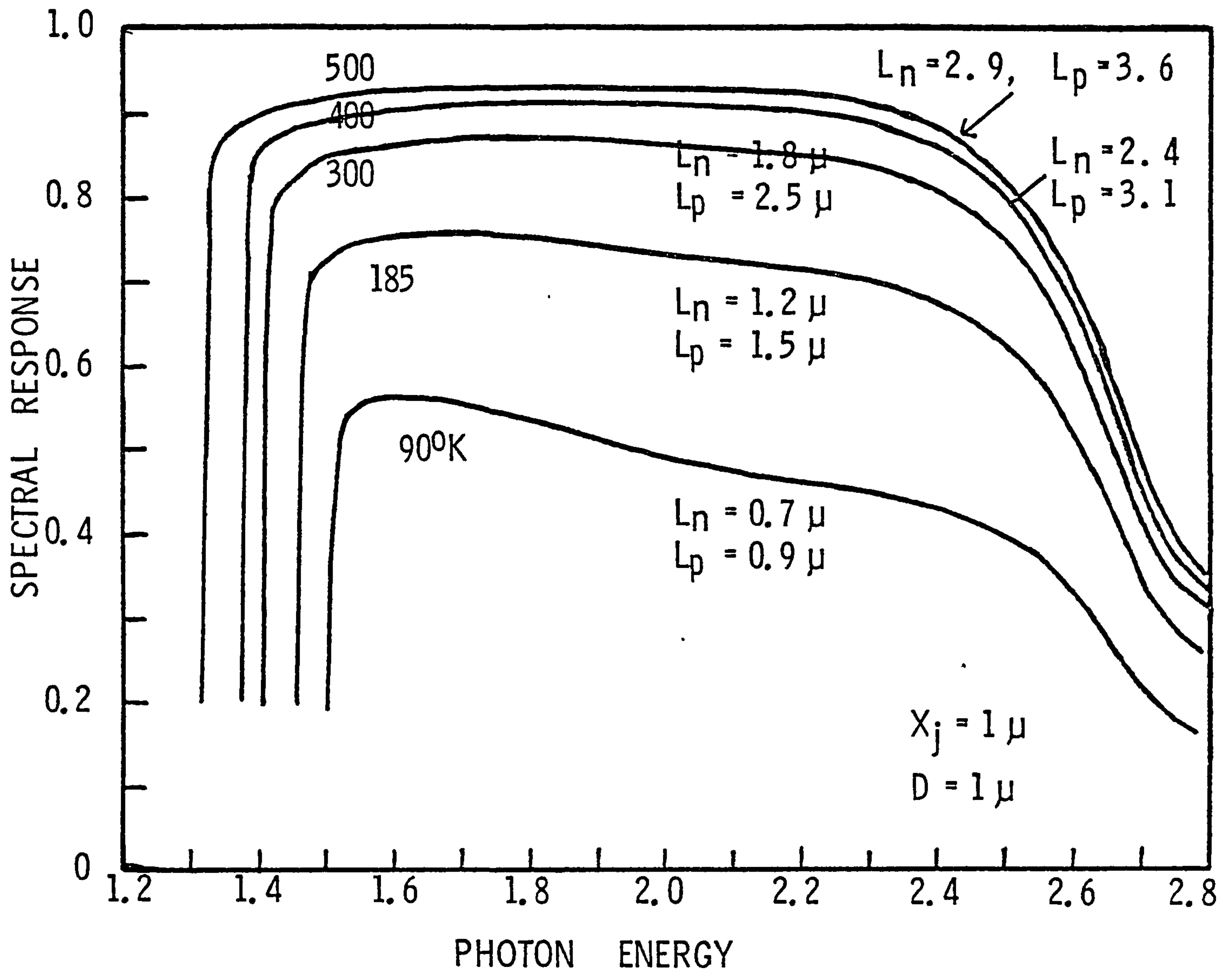

CALCULATED RESPONSES OF CELLS WITH MODERATE JUNCTION DEPTHS

Figure 10

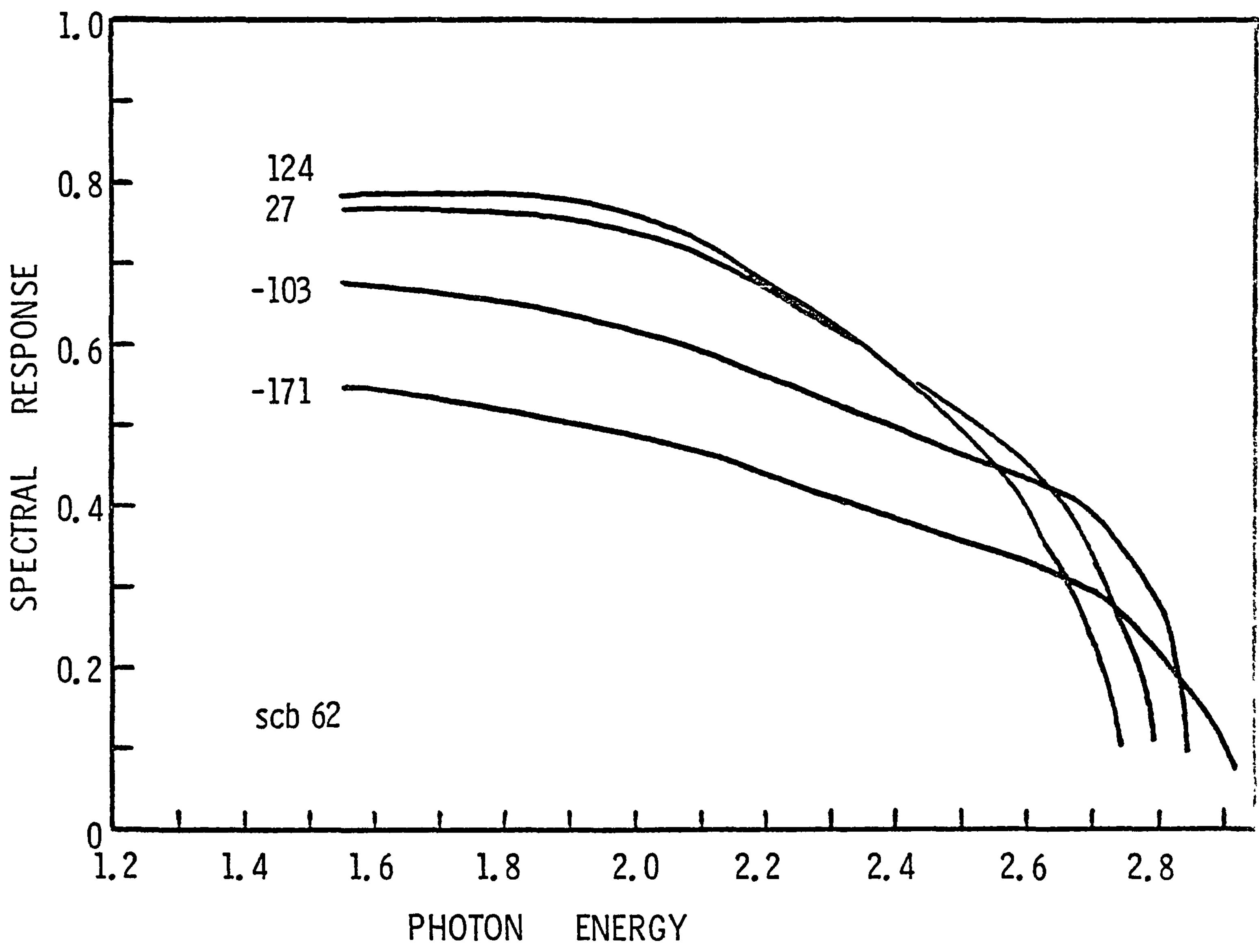

Figure 11

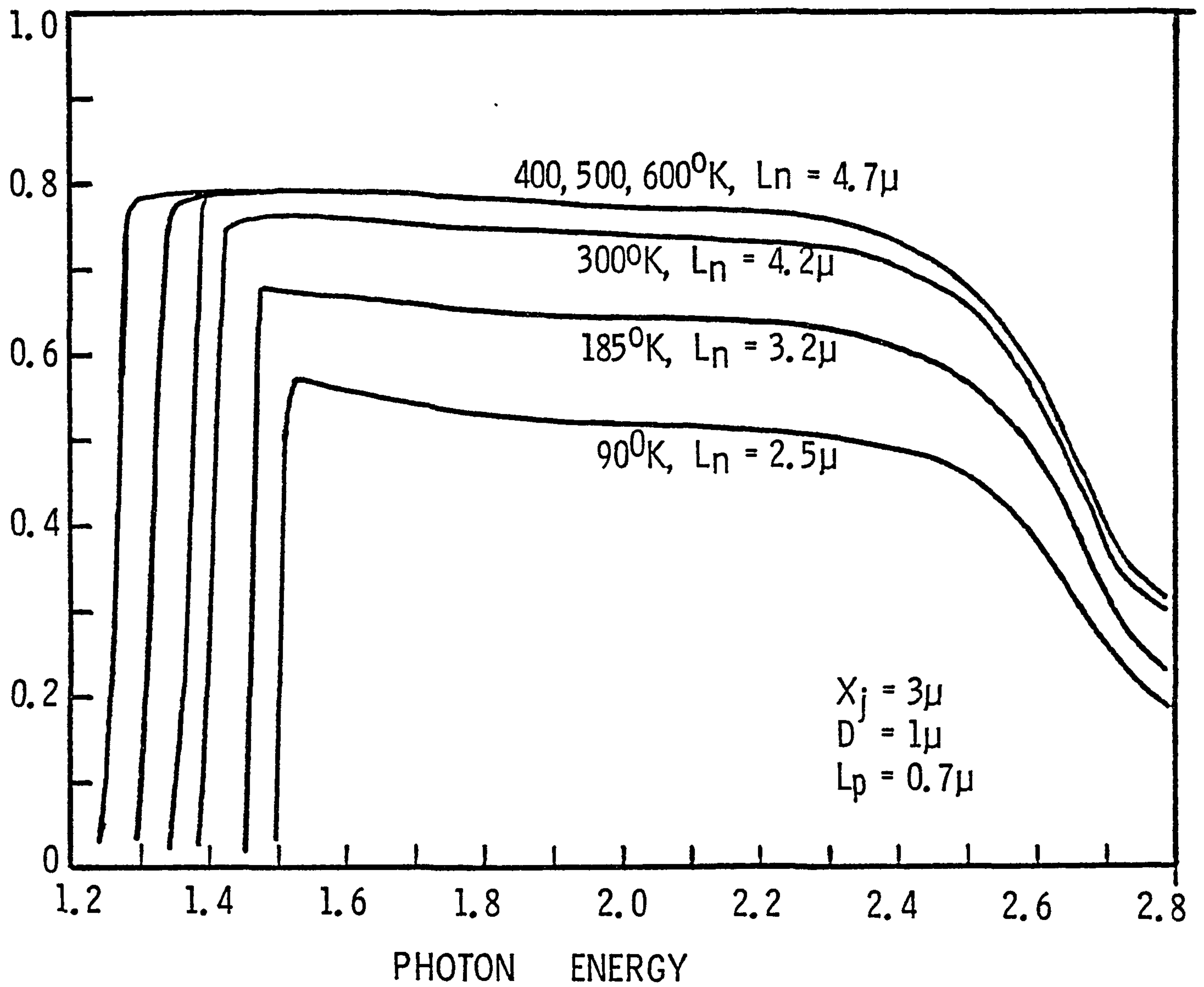

CALCULATED RESPONSES, DEEP JUNCTIONS

Figure 12

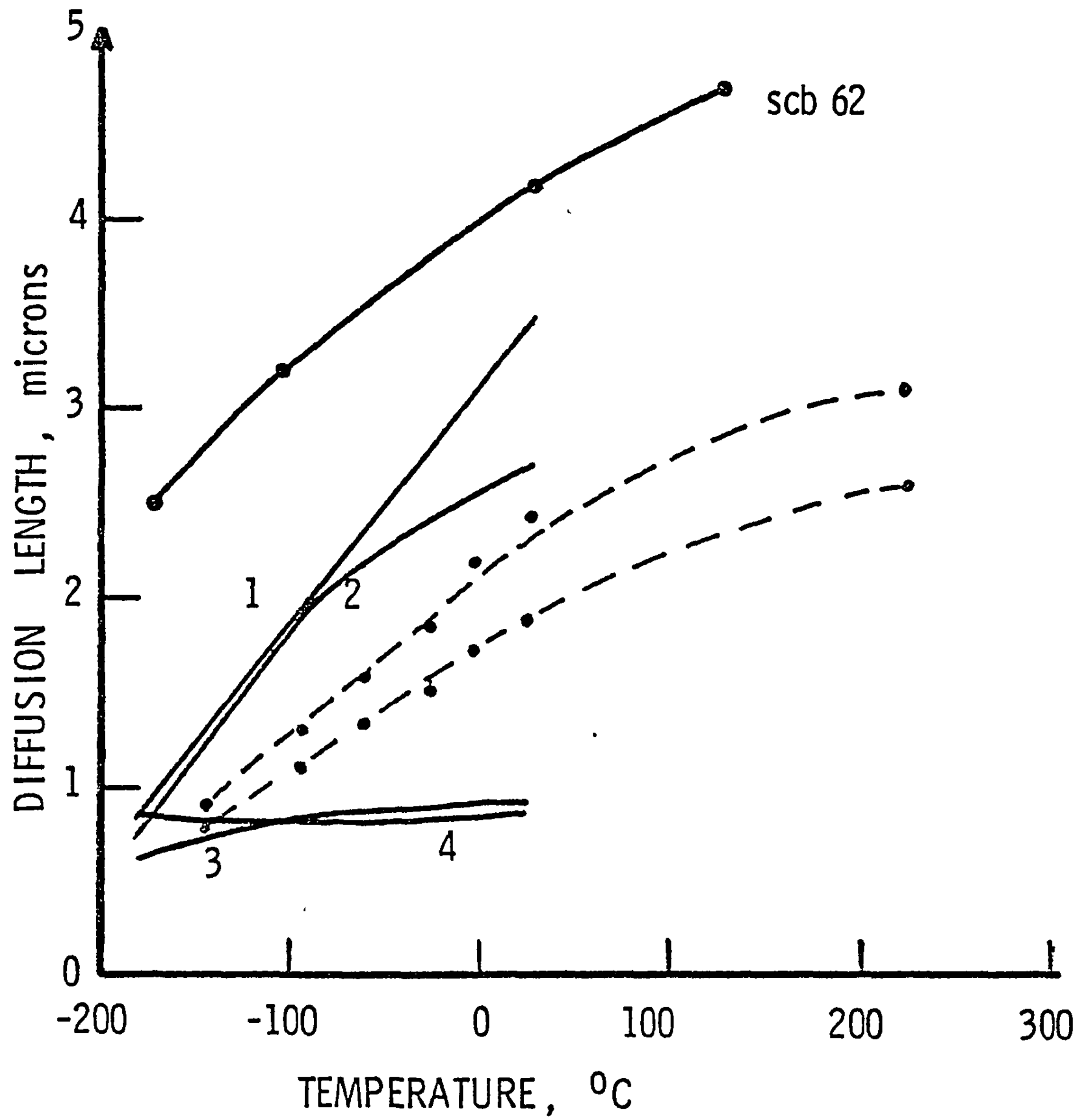

1. L_n. $N_a = 6\times10^{17}$
2. L_n. $N_a = 2\times10^{18}$ ref. 5
3. L_n. $N_a = 1\times10^{18}$

4. L_p. $N_d = 2\times10^{18}$ ref. 7

Diffusion length versus temperature.

Figure 13

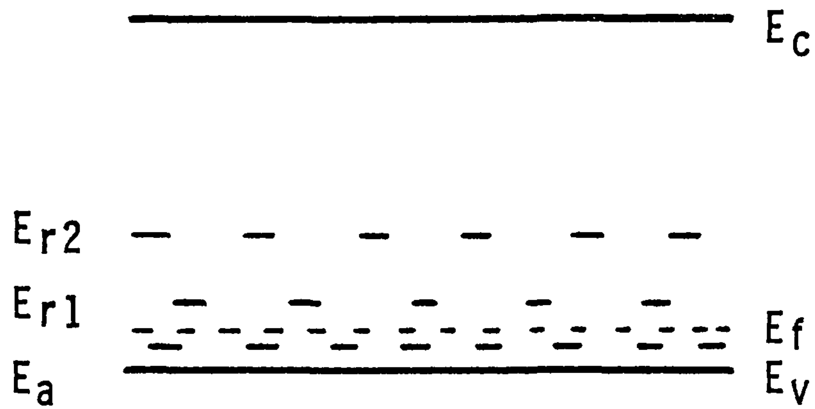

Energy band diagram, shallow
and deep recomb. centers.

Figure 14

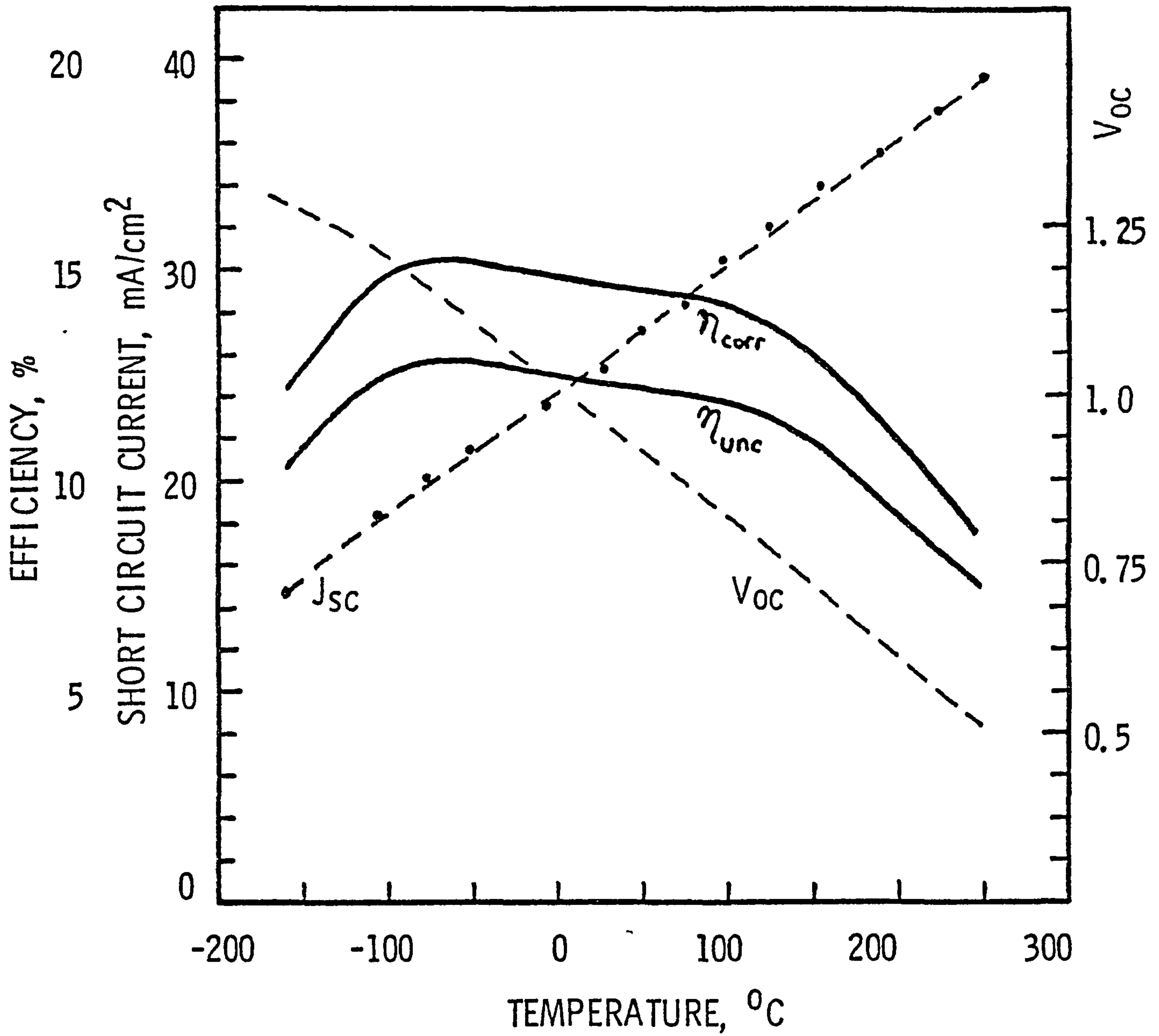

Open circuit voltage, short circuit current, and efficiency under Xenon light (135 mW/cm^2).

Figure 15

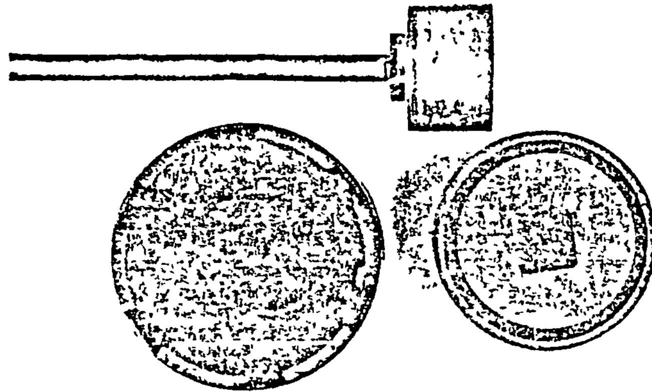

(a)

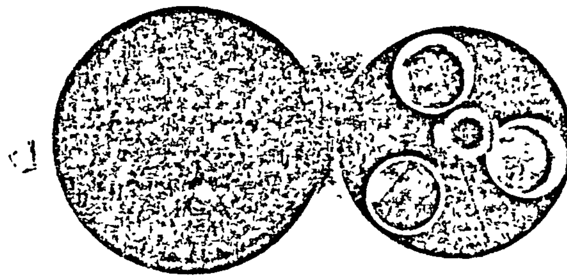

(b)

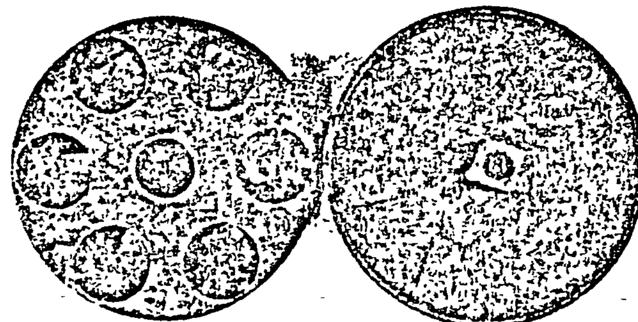

FIGURE 1 - Ref. 1

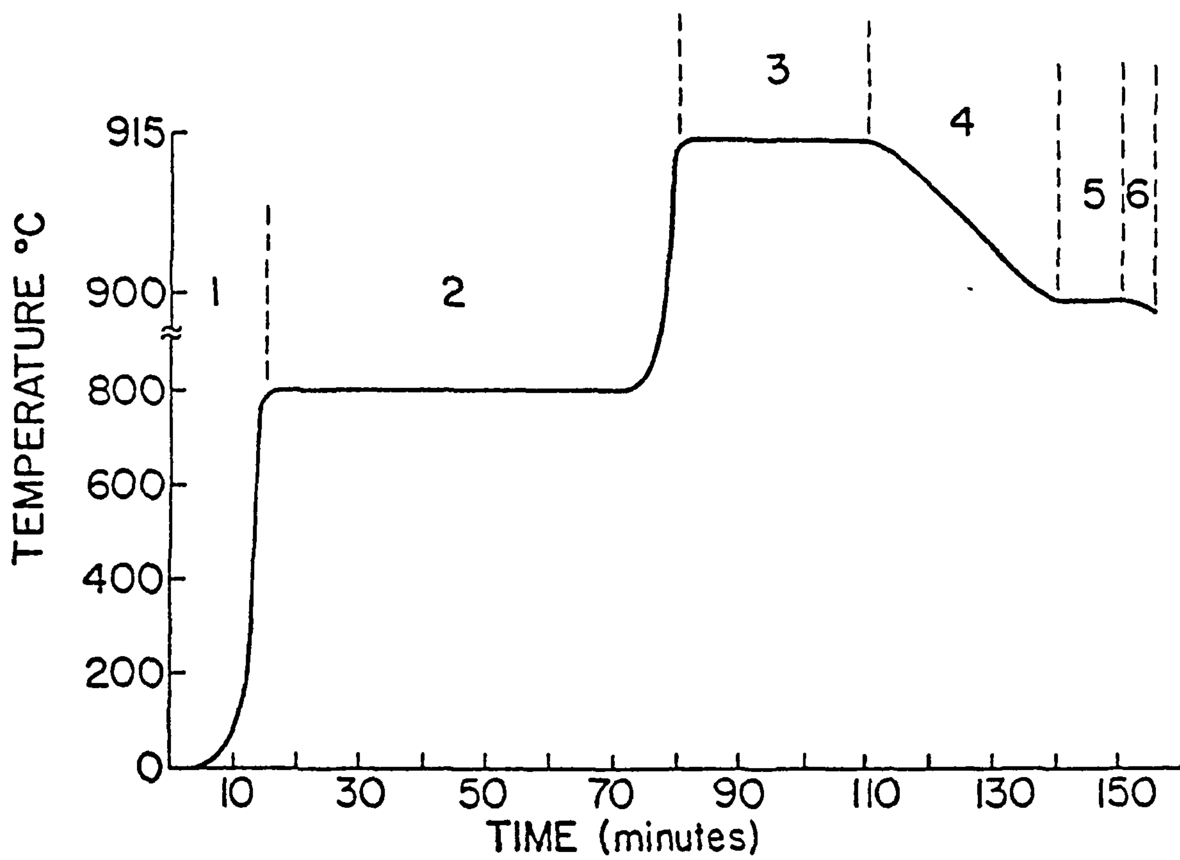

Figure 4 - Ref. 1